Numerical computations of hypersonic boundary layer roughness induced transition on a flat plate

Gennaro Serino *, Fabio Pinna †and Patrick Rambaud ‡

von Karman Institute for Fluid Dynamics, Chausse de Waterloo 72, B-1640 Rhode-St-Genese, Belgium

The work is focused on numerical simulations of roughness induced transition for hypersonic flow on a flat plate wall mounted roughness element. Numerical simulations are compared to experimental results in order to resemble the physics highlighted in the tests. In particular, stress has been placed on the detection of the vortices in the wake behind the roughness element and on the onset of transition.

I. Introduction

Since the experiment of Reynolds in 1883, the scientific community has demonstrated a great interest in transition to turbulence due to its influence on crucial fluid dynamic quantities such as drag and heat transfer. In high subsonic conditions, keeping the flow laminar on a commercial aircraft wing means reduction of drag and fuel consumption with substantial cost savings. In addition, higher heat flux in case of turbulent flow makes transition prediction crucial for the survival of the vehicle and of the crew during a re-entry at hypersonic speed.

The mechanism of transition is influenced by several parameters which can be related both to free stream conditions, as the noise or turbulence level, and to the body itself, as the presence of surface irregularities or vibrations. Linked to the originating cause of disturbances, there are several path which actually leads to transition (Reshotko[1]). For small enough disturbances we usually observe *natural transition* through different well defined stages (White[2]). When initial disturbances entrained in the boundary layer are sufficiently strong, all these stages could be by-passed leading to a much quicker transition to turbulence. The latter case is defined by Schlichting[3] as *bypass transition* as opposed to the mechanism of linear amplification of unstable waves (Morkovin[4]) which characterizes *natural transition*.

When transition is caused by surface irregularities, it is defined as *Roughness Induced Transition* (hereafter RIT) and it plays a crucial role in space applications as, during re-entry, misaligned tiles or undesired gaps may promote turbulent flows with a following increase in heat flux and an abnormal wear of the heat shield. The understanding of the physics of RIT has sensibly improved in these years thanks to numerous experimental investigations as those reviewed by Ergin and White.[5] In many of the cases observed by them, around an isolated three dimensional roughness element, the flow showed similar and repetitive structures. Upstream of the obstacle (a cylinder or a diamond roughness element), a steady horseshoe vortex was observed going around the element and wrapping it while, on the lateral parts, two steady counter-rotating legs were observed. The steady vortices (*first generation*) rapidly evolved downstream into streaks of low or high intensity whose footprints can be obtained with oil-sublimation or infrared thermography visualization techniques. The transition location is generally recognized in experiments where the turbulent wake starts to widen with an half angle of 10° respect to the flow direction as it can be seen in Fig. 1. Finally, when the Reynolds number is sufficiently high, as in hypersonic conditions, unsteady vortices (*secondary generation*) originate from the separation region in the back of the roughness element accelerating the transition mechanism.

In parallel with experiments, numerous efforts have been put in *Computational Fluid Dynamics* (hereafter CFD) in order to develop a valid transitional model capable of reproducing the physics of RIT. The importance of this numerical tool relies in the possibility to predict transition and its effect, as the increase in the

*PhD Candidate, Aerospace Department, gennaro.serino@vki.ac.be, AIAA Student Membership

†PhD Candidate, Aerospace Department, fabio.pinna@vki.ac.be

‡Assistant Professor, Aerospace Department, patrick.rambaud@vki.ac.be

heat flux. In hypersonic applications, this would allows to design with less conservative safety factors which are commonly used in the *Thermal Protection System* (hereafter TPS) resulting in cost savings, in more space for the payload and, mainly, in higher probabilities of success.
The state of the art on numerical simulations on RIT is represented, among others, by the efforts of the NASA research team led by M.Choudhari. In one of his most recent work,[6] a parametric study on the roughness height is carried out with the NASA CESE algorithm which is a second-order accurate scheme in space and time. Stress is placed on the description of the unsteadiness of the wake behind the cylindrical roughness element and it has been shown that when the height to the boundary-layer thickness ratio exceeds 0.8, wake instability occurs due to the front-side separation region. Results of the simulations show agreements with experiments but the high computational cost makes the approach unsuitable for an engineering transition prediction applicable at larger scales (simulations on the full vehicle configuration). A research team of the *Italian Aerospace Research Center* (CIRA) led by R. Donelli[7] presents an interesting approach in laminar to turbulent transition in hypersonic flows. Transition mechanism is investigated on a blunt cone with a parametric analysis on the leading edge radius, the Reynolds number and the Mach number. The purpose is to build up a potential surface to apply in experimental investigations in order to predict influences of the parameters in such experiments. The approach is promising and suitable for industrial applications but an experimental validation is still missing.
Roughness induced transition has been deeply investigated at von Karman Institute for Fluid Dynamics (hereafter VKI) mainly by an experimental point view. Tirtey[8] presents the study of the flow-field structure in the vicinity and in the wake of an isolated 3D roughness element. Different experimental techniques have been coupled and supported by CFD simulation for a good understanding of the flow-field topology. Both experimental and CFD simulations have shown similarities for different roughness elements.
Although *solving is not understanding*, the objective of the current work is to use a commercial package to reach a level of simulation comparable with the experimental database available at the VKI in order to not only improve the understanding of the physics of RIT, but also to have a valid tool for an engineering transition prediction applicable in hypersonic conditions.

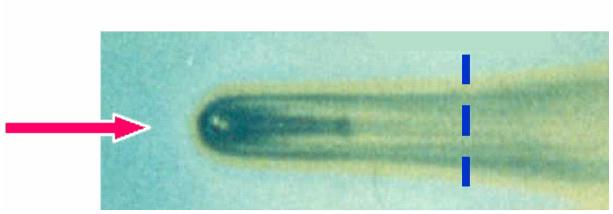

Figure 1. Transition induced by an isolated roughness element (transition onset at dashed blue line)[5]

II. Experimental Setup

Experiments described by S.Tirtey[8,9] have been carried out in the VKI hypersonic tunnel H3. It is an open loop blow-down facility supplied by high pressure air, feeding an axisymmetric nozzle that provides a Mach 6 free jet 12 cm in diameter. The test gas passes through a pebble-bed heater, which supplies air at temperature ranging from ambient to 550 K and pressures ranging from 7 to 35 bar. Unit Reynolds number may be varied from $9 \times 10^6(m^{-1})$ to $30 \times 10^6(m^{-1})$. The test section contains a three-degree-of-freedom traversing system for model or probe support that also allows the angle of incidence to vary between $\pm 5°$. Three H3 standard conditions(low, medium and high Reynolds numbers) have been defined and are summarized in Tab. 1:

Table 1. VKI H3 wind-tunnel standard conditions

Conditions	$P_0(Bar)$	$T_0(K)$	Unit Reynolds m^{-1}	Mach
Low Re	11	500	$9.2 \cdot 10^6(m^{-1})$	6
Medium Re	21	500	$1.8 \cdot 10^7(m^{-1})$	6
High Re	31	500	$2.6 \cdot 10^7(m^{-1})$	6

High Reynolds conditions are those used in the current computations and experimental results are compared with the numerical simulations. In the experiments carried out by Tirtey,[8] several roughness geometries have been considered. First, the ramp roughness element has been chosen since there is no stagnation point on the front region and there is no overheating. Nevertheless, real surface unevenness are also due to bumps, cavities, steps and misaligned tiles which can be modeled through spherical, cylindrical and squared roughness elements. In Fig. 2 and Fig. 3 a scheme of the flat plate used for the tests in the VKI H3 wind tunnel and the different roughness geometries with relative dimensions are respectively represented. The conditions of the computations are those indicated as *High Reynolds* in Tab. 1.

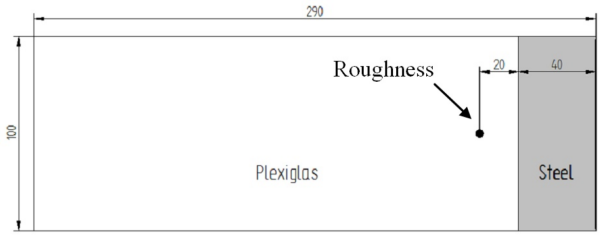

Figure 2. Top view schematic of the flat plate for H3 testing

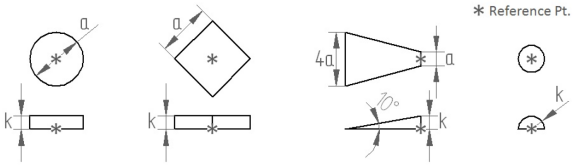

Figure 3. Roughness geometries : cylinder, diamond, ramp and half-sphere elements

Experiments have highlighted two main generations of vortices in the wake of the roughness element as schematically represented in Fig. 4 and described by Ergin.[5] In Fig. 4(a) the *primary generation* is represented in the part of the wake close to the axis of symmetry while in Fig. 4(b) is is shown that the *secondary generation* contribute to the widening of the wake due to high speed streaks propagating downstream. The physics has been deduced via interpretation of the experimental footprint obtained with different techniques described by Tirtey[8] such as the infrared thermography shown in Fig. 4(c). Numerical simulations aim at reproducing the same physics by resembling both generations of vortices.

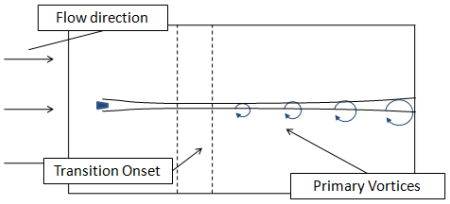

(a) Primary generation of vortices

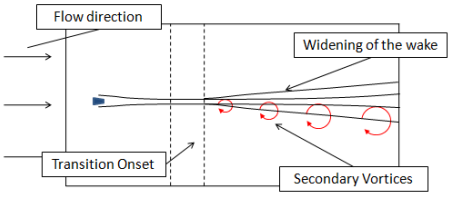

(b) Secondary generation of vortices

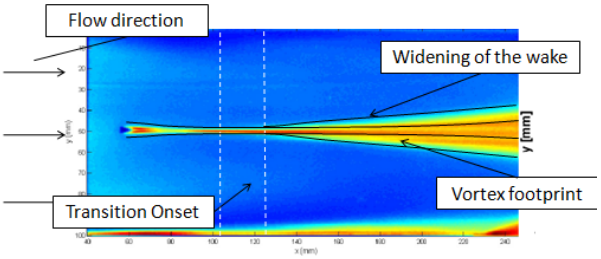

(c) Experimental vortex footprint[8]

Figure 4. Schematic representation of the physics highlighted in the tests

III. Transitional models

Despite the fact that transition is an inherently unsteady phenomenon, researchers propose transition models where relations should return the behavior of a transitional boundary layer, feeding this results in a standard CFD code. Of course, as it happens in *Reynolds Average Navier Stokes* (hereafter RANS), their validity is limited, nevertheless this approach could lead to some results, especially for quantities like heat flux and skin friction, at least from an engineering point of view. In the work of McKeel[10] a series of existing RANS models is discussed and implemented, ranging from Baldwin-Lomax to standard Wilcoxs $k-\omega$. Also the Schmidt & Patankar modification to low-Re $k-method$ was investigated, along with the one equation turbulence model accounting for first and second mode developed by Warren, Harris and Hassan.[11] Also both the algebraic model of ONERA/CERT and the one from Dey and Narashima, which linearly blends the laminar and turbulent field through intermittency to simulate the transition region, have been analyzed by McKeel.[10] All these models showed some sort of drawbacks, relying on a dedicated tuning for a correct prediction of transition.

Other approaches, like the one of Sieger et al.,[12] were based on empirical correlations to determine the start and ending transition Reynolds numbers. These were used to compute, together with the Reynolds number based on the local boundary layer thickness, the intermittency value. The development of Langtry,[13] in 2006 used a transport equation for the intermittency. This is not a novelty in itself as a series of models have been developed around this idea; the strong point of this approach is the use of local variables together with correlations, resulting in a good match for many cases. It has to be noted that, as the model relies on correlations, it still lacks of general validity. Another interesting approach has been recently proposed in the work of Mayle & Schulz[14] where the laminar kinetic energy is transported. The breakdown to turbulence happens, according to this model once the laminar fluctuations reach a threshold level. This method has been recently reformulated by Walters & Leylek[15] to transport this quantities locally, making the model ready to be used along with normal CFD applications. Both Langtry's[13] and Walters'[15] models are originated in the turbo machinery community and application to hypersonic flows is somehow not recommended without tweaking them. Moreover, the special features of hypersonic testing, make difficult the access to the correlations data, needed to recalibrate these models, and more work will be needed in the future.

The code used for the work is the commercial package of CFD++[17] in which a transitional model is implemented. This model is referred to as the $R-\gamma$ model based on two transport equation for the undamped eddy-viscosity (R) and for the intermittency factor (γ) defined as the turbulent-laminar flow time ratio. The model is based on the work of Ryong[16] who exploits the transport equation for the eddy viscosity (R) of Goldberg[18]'s one-equation turbulence model that is similar in form to the model of Spalart-Allmaras.[19] The equation is coupled with the transport equation for the intermittency factor that, by definition, is the time fraction in which a region is interested by a turbulent spot. Therefore, according to local value of γ, the production terms in the eddy viscosity equation are activated or damped in order to trigger transition mechanism. In the solver, the initial condition on the free-stream eddy viscosity is indirectly set by varying the turbulent/laminar viscosity ratio ($VR = \mu_t/\mu_\infty$). Further details on the model are reported in sections III.A and III.B.

III.A. Eddy viscosity (R) transport equation

The undamped eddy viscosity R is defined as follows

$$R = \frac{\mu_t}{f_\mu \rho} \tag{1}$$

where f_μ is a low Reynolds number damping function that can be found in the manual of $CFD++$.[17]

$$\frac{D(\rho R)}{Dt} = \frac{\partial}{\partial x_j}\left[(\mu+\mu_t)\frac{\partial R}{\partial x_j}\right] + \rho(C_1 + C_2 f_2 f_\gamma)(RP_k)^{0.5} - \rho C_3 D \tag{2}$$

where P_k is the rate of turbulence production defined as follows

$$P_k = \nu_t\left[\left(\frac{\partial U_i}{\partial x_j}+\frac{\partial U_j}{\partial x_i}\right)\frac{\partial U_i}{\partial x_j} - \frac{2}{3}\left(\frac{\partial U_k}{\partial x_k}\right)^2\right] \tag{3}$$

while f_2 and f_γ are respectively specialized near wall and intermittency gradient functions. Finally C_1, C_2, C_3 are model constant defined as

$$C_1 = 21.479 \quad C_2 = 21.394 \quad C_3 = 1.5 \tag{4}$$

III.B. Intermittency (γ) transport equation

The intermittency factor γ is defined as the fraction of time in which the flow is turbulent respect to its laminar state. The transport equation for such variable is the following

$$\frac{D(\rho\gamma)}{Dt} = \frac{\partial}{\partial x_j}\left\{[\mu + (1-\gamma)\mu_t]\frac{\partial \gamma}{\partial x_j}\right\} + \rho\gamma(1-\gamma)\sqrt{\frac{0.09P_k}{R}}(1.6 - 0.16\Gamma) + 0.15\mu_t\frac{\partial\gamma}{\partial x_j}\frac{\partial\gamma}{\partial x_j} \tag{5}$$

where Γ is defined as

$$\Gamma = \frac{(R/0.09)^{1.25}}{P_k^{0.75}}\frac{U_i}{\sqrt{U_l U_l}}\frac{\partial U_i}{\partial x_j}\frac{\partial \gamma}{\partial x_j} \tag{6}$$

IV. Computational domain

The numerical scheme is a point-wise implicit second order finite volume which is applied to a 10^7 hexahedral cells structured mesh after a sensitivity study on the grid. The computational domain consists of a 0.5 mm round nose and 30 cm length flat plate with a 0.8 mm height ramp roughness element placed at 54.5 mm respect to the leading edge as shown in Fig. 5. In order to save computational cost, only half of the physical domain has been simulated and the symmetry condition has been applied on the $x - z$ plane cutting the geometry in half.

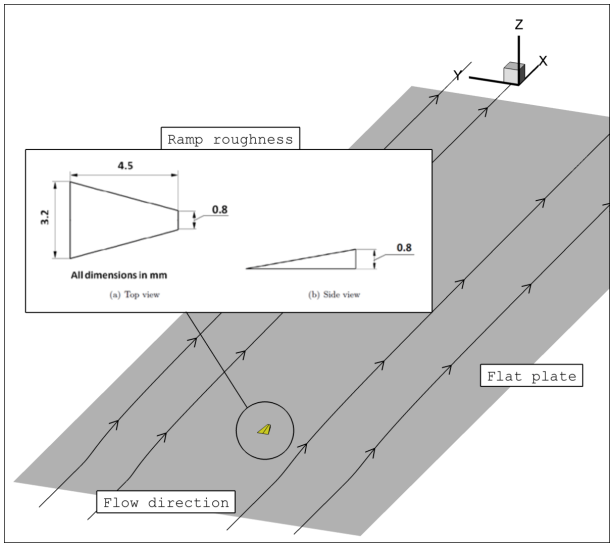

Figure 5. Computational domain and ramp roughness element

Initial conditions resemble the values at which experiments were performed in the VKI H3 wind tunnel (High Reynolds) thus having a free stream Mach number equal to 6 as indicated in Table. 2.

Table 2. Initial Conditions

P (Pa)	U (m/s)	T (K)	VR	R (m^2/s)	γ
1936.42	939.15	60.976	2	$7.2123e^{-5}$	0.1

A detached normal shock wave is generated on the flat plate round leading edge while it gradually degenerates into a Mach wave ($\mu = \arcsin 1/M_\infty = \arcsin 1/6 \approx 9.6°$) by approaching further downstream. The shock is captured through a shock fitting approach consisting in resembling the shape of the shock wave with a proper mesh density as it can be noticed in Fig. 6(a). Moreover, as most of the physics occurs around the roughness and its wake, a bounding box around the ramp is used to properly solve the three dimensional-separated flow field, as well as the separated induced weak shock on its backward facing step, as shown in Fig. 6(b). Finally, a higher mesh density is used to solve the wake in order to capture both generations of streaks which propagate downstream.

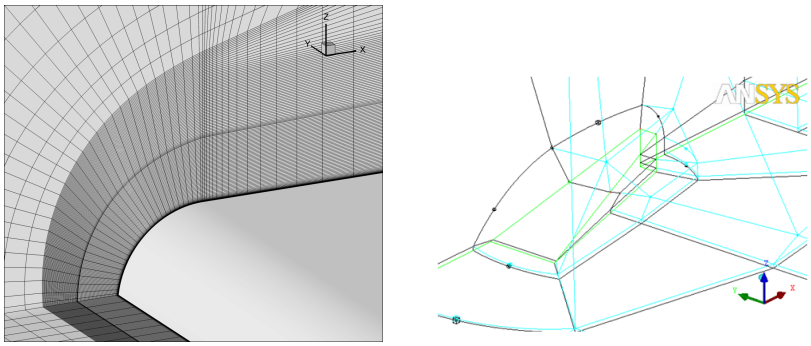

(a) Shock fitting (leading edge) (b) Bounding box (ramp element)

Figure 6. Details of the computational mesh

V. Assessment of the Transitional Model

Several simulations have been carried out to study the influence of different parameters. Initial conditions on the viscosity ratio (VR) and on the intermittency factor (γ) have been varied to study the influence of the $R-\gamma$ transitional model on the solution in term of transition onset location. Additionally, the mesh density has been progressively increased to study the effects on the resolution of streaks in the wake. The criterion of variation of the parameters has been the comparison between the numerical solution and the experimental results of Tirtey.[8]

The viscosity ratio (VR) has been varied in order to match the experimental transition onset location by progressively decreasing the initial value at the inflow from 4 to 1. In Fig. 7(a) the skin friction coefficient ($c_f = 2\tau_w/\rho_\infty V_\infty^2$) is plotted on a plane far enough from the wake induced by the roughness element in order to detect natural transition onset on the flat plate. The natural transition onset location is where the c_f increases respect to the laminar solution towards the turbulent solution. A $VR = 4$ has determined a fully turbulent flow while, by progressively reducing the viscosity ratio, a transitional flow is obtained with the natural transition onset location moving downstream. A $VR = 1$ allows to have a laminar flow. The *bump* which is observed in the plotting is probably due to the structured mesh used for the roughness to describe its geometry.

The skin friction coefficient has been plotted in a plane inside the wake in Fig. 7(b) in order to detect bypass transition. Results have been compared to two dimensional Haas'[20] simulations for different viscosity ratios. Transitional flow in the wake is obtained for a $VR = 2$, so that this value has been used for the current work even if natural transition, not observed in the experiments, occurs on the flat plate further downstream

The viscosity ratio has an influence on the evolution of the vortices downstream of the roughness. In fact, recalling that $VR = \mu_t/\mu_\infty$, the higher is the viscosity ratio the higher is the turbulent viscosity and the higher is the dissipation introduced in the domain. This results in vortices which are quickly damped and less defined on the outlet plane as it can be noticed in Fig. 8(a) compared to Fig. 8(b).

Further investigations involved the effect of the intermittency factor γ and of the mesh size.

The manual of $CFD++$[17] recommends to set the intermittency factor γ to 0.1 as initial condition on the inflow as did in the investigation on the variation of the viscosity ratio. Therefore, several values have been used to study the effects of this parameter on the results. No significant effects have been observed on the solutions in term of transition onset by varying the initial condition on γ free stream value. In fact, by

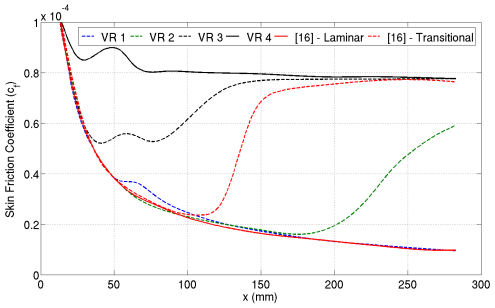

(a) out of the wake ($y = 45$ mm)

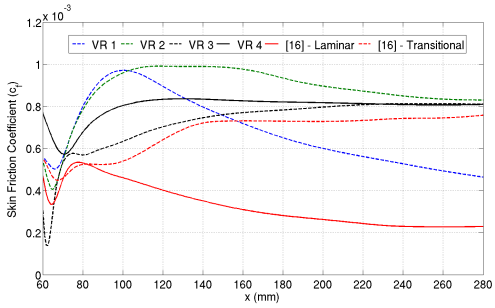

(b) in the wake ($y = 0$ mm)

Figure 7. Skin friction coefficient on cut planes

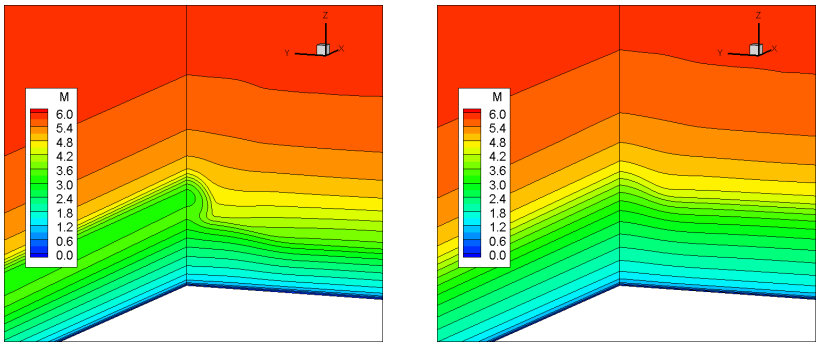

(a) $VR = 2$ (b) $VR = 4$

Figure 8. Visualization of the vortex on the outlet plane (Mach number contour)

setting a theoretically fully laminar ($\gamma = 0$) and fully turbulent ($\gamma = 1$) flow at the inlet, results resemble those previously obtained for $\gamma = 0.1$. The reason is that, in the $R - \gamma$ transitional model, the effect of the viscosity ratio overcomes the coupling effect of the intermittency transport equation as it can be seen by the production term P_k in Eq. 3 which makes Eq. 5 dependent on the turbulent viscosity μ_t.
Keeping $VR = 2$, the influence of the mesh size has been investigated by increasing the number of cells from 6.5×10^6 to 10×10^6. Vortex resolution is clearly higher as shown in Fig. 9(a) and Fig. 9(b), since the interpolation between neighborhood elements allow to describe gradients with less dissipation on the numerical solution. On the other hand, transition occurs earlier in the wake when the number of cells is larger, without natural transition occurring on the flat plate as represented in Fig. 10(a) and Fig. 10(b). In addition, the width of the wake is reduced when the density is increased since gradients are better solved at the wall as previously observed for the vortices on the outlet plane.

Finally, in Fig. 11, the effect of the viscosity ratio on the transition onset and on the width of the wake is represented. It is possible to define a quasi-linear relation between the natural/bypass transition onset and the viscosity ratio while, by increasing the VR, the natural and the bypass transition onset get closer until a fully turbulent flow occurs at $VR = 4$. The viscosity ratio has an effect on the wake width which corresponds to a linear increase in the range going from $VR = 1$ to $VR = 3$, while the growth of the wake width is reduced at $VR = 4$, probably because of the higher dissipation introduced by that value. Therefore, we can conclude that for the current case the proper value of the viscosity ratio of the $R - \gamma$ transitional model has to be set between $2 \div 3$ in order to have transitional flow in the wake. Moreover, when the viscosity ratio is equal to 2, results are closer to the experiments so that $VR = 2$ has been used for the current simulations for a qualitatively comparison with results of the tests.

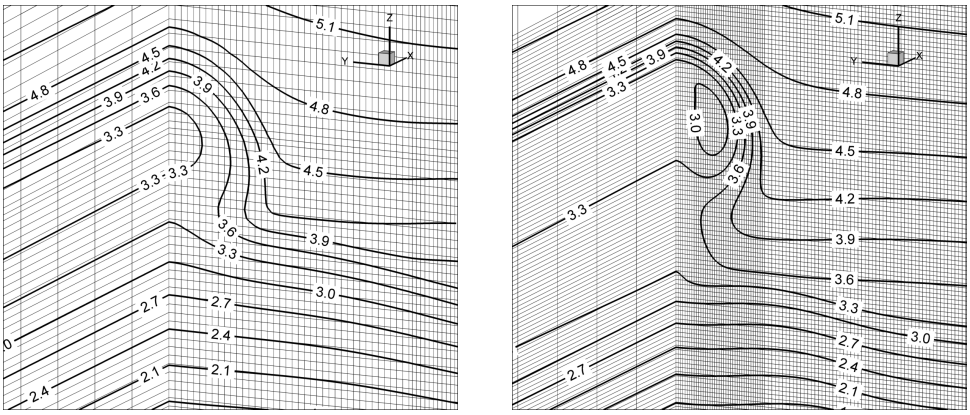

(a) 6.5×10^6 cells (b) 10×10^6 cells

Figure 9. Resolution of the vortex on the outlet plane (Mach number contour)

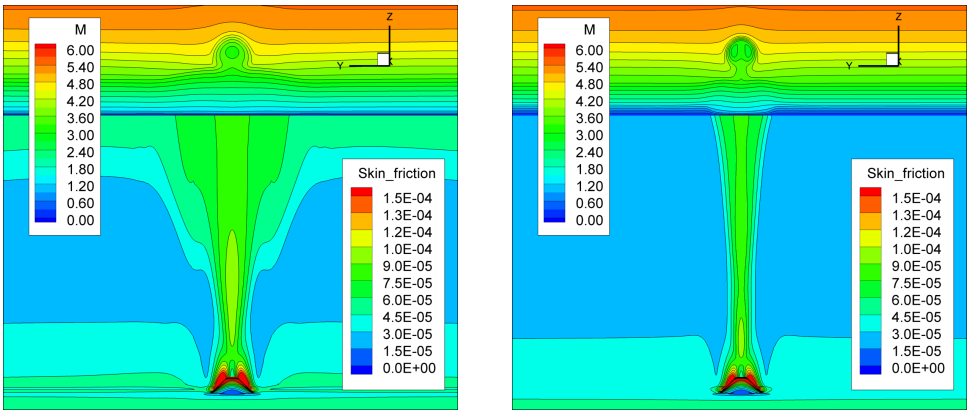

(a) 6.5×10^6 cells (b) 10×10^6 cells

Figure 10. Wake downstream of the roughness element : Mach number (outlet plane) and Skin friction (wall) contour)

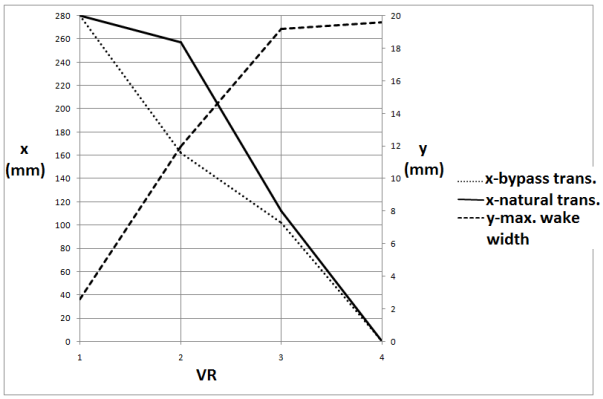

Figure 11. Effects of the viscosity ratio on transition onset and wake width

VI. Numerical Results

VI.A. Ramp roughness element

Despite of the great influence of the viscosity ratio and of the mesh size, the $R-\gamma$ transitional model has demonstrated interesting results. In particular, the skin friction pattern is described in a detailed and high resolution way so that an interpretation of the flow could be given in the light of the critical point theory of Poincarè. In Fig. 12(a), the flow topology around of the roughness element os represented by considering the skin friction lines and the corresponding critical points. In particular, in the fore part, the flow leaves the surface at the saddle point S_1 and it reattaches on the node N_1. In the rear zone, the flow detaches from the surface at the foci F_1 and F_2 and on the saddle points S_2 and S_3. Finally, reattachment occurs in the wake in correspondence of the node N_2. In Fig. 12(b) converging skin friction lines can be observed on the lateral side of the wake so that, according to the critical points theory, there is flow lifting off the surface and wrapping around generating vortical structures. On the contrary, skin friction lines are diverging in the central part of the wake (Fig. 12(c)) implying a flow reattachment on the wall.

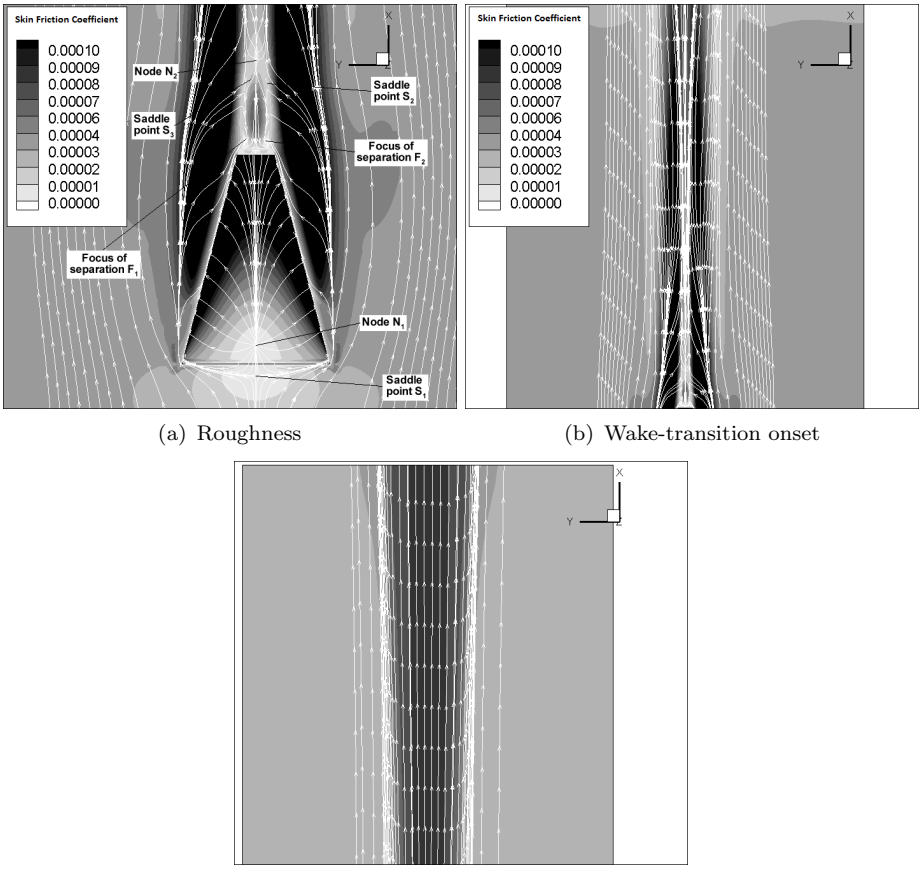

(a) Roughness

(b) Wake-transition onset

(c) Wake-downstream

Figure 12. Skin friction patterns and lines

Vortices have been identified by applying standard criteria as the $Q-Criterion$ and by considering the vorticity magnitude as well as the helicity as described by Batchelor.[21]
The Q-criterion is a vortex identification criterion based on Galilean-invariant which defines a vortex as a spacial region where $Q = 1/2[|\Omega|^2 - |S|^2] > 0$ that is where the Euclidean norm of the vorticity tensor(Ω) dominates that of the rate of strain(S). On a practical side, the threshold value can be considered greater than 0. In fact, in current simulations, this value has been progressively increased until the vortices were isolated and clearly distinguishable. In historical order, the first three dimensional vortex criterion using the velocity gradient decomposition is the Q-criterion of Hunt, Wray and Moin (1988). In Fig. 13(a), the two steady vortices are highlighted in the central part of the wake while the secondary lateral vortices

progressively disappear downstream. We can conclude that primary vortices carry more energy than the secondary ones and that the mesh is capable of capturing both of them. Around the roughness element, the lateral counter rotating legs cited by Ergin,[5] are identified through the $Q - criterion$ even if the shape is not enough resolved mesh.
Helicity is then represented in Fig. 13(b) to highlight the vortices generated in the wake at several distances behind the roughness element. As it is represented, the vortices are lifting off the surface leaving their footprint highlighted by the skin friction coefficient contour at the wall. Vortices in the central part of the wake are stronger so that they survive for a longer distance respect to the lateral structures which are quickly damped approaching downstream.

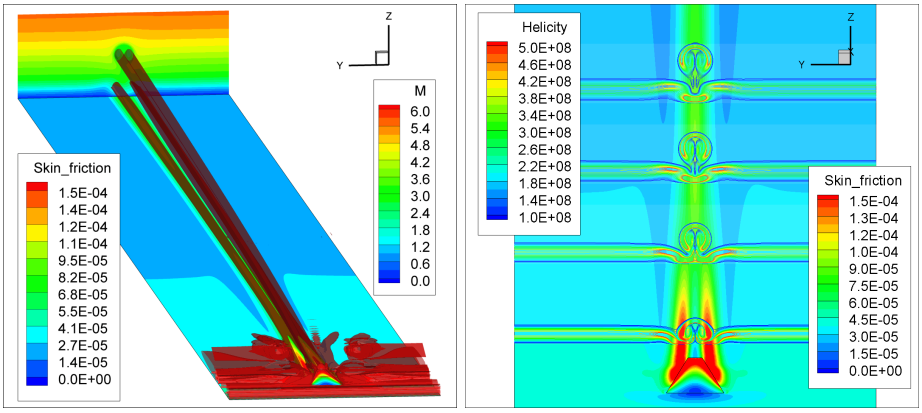

(a) Q isosurfaces (b) Helicity isolines

Figure 13. Vortex identification : Mach number (outlet plane) and skin friction (wall) contours

The comparison with the experiments has been carried out on a smaller region of the computational domain by creating a "box" (Fig. 14) containing the roughness and its wake and using a 10^7 cells. The primitive variables computed in the global simulation have been interpolated on the inlet plane as well as on the "roof" of the box domain to be used as boundary conditions.

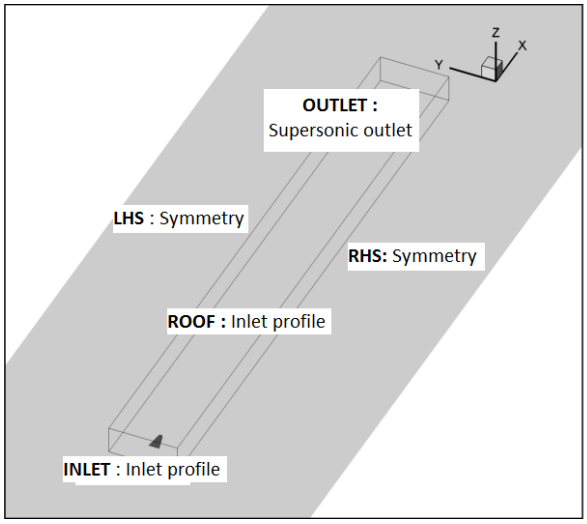

Figure 14. *Box* **domain surrounding the roughness and its wake : geometry and boundary conditions**

Current numerical simulations have been qualitatively compared to the "High Reynolds" condition of Tab. 2 by means of of the skin friction pattern and the wall heat flux.
The latter is obtained in the experiments with a sublimation technique and it is shown along with numerical results in Fig. 15. The skin friction line patterns distribution is experimentally obtained by means of an oil visualization technique and it is compared with numerical results in Fig. 16.

For both these quantities, the topology obtained with numerical simulations is very close to the experimental one on the lateral and rear part of the roughness element since lateral steady vortices touch the wall with the same footprint as the experimental one. Also, the numerical onset of transition qualitatively matches the test results. On the other side, the numerical simulation misses the secondary generation of vortices for such a resolved mesh, so that, downstream of the transition point, the wake is narrower.

Figure 15. Heat flux experimental(bottom)-numerical(top) distributions comparison

Figure 16. Skin friction experimental(bottom)-numerical(top) distributions comparison

VI.B. Other roughness geometries

Other roughness geometries have been analyzed with the $R-\gamma$ transitional model in order to test whether conclusions drawn for the ramp roughness element could be applied generally. These geometries include a diamond, a cylinder and an half-sphere as represented in Fig. 3. Numerical simulations have been carried out considering the same viscosity ratio ($VR = 2$) already used for the ramp roughness geometry to evaluate the transitional model reactions to different geometries. A smaller section (a *box*, Fig. 14) of the computational domain surrounding the roughness and its wake has been considered for these geometries in order to increase the resolution of results and to try to capture the physics of the experiments. At the inlet of the *box*, the primitive variables obtained by the simulation for the ramp roughness element with $VR = 2$ has been considered. The inlet has been set far enough with respect to the roughness element, in order to allow the flow to relax and adapt to the new conditions. Nevertheless, attempts to vary the VR inside the box revealed slight variations of the results since, as already discussed, the $R-\gamma$ transitional model is very sensitive to initial conditions and, in particular, to the initial level of turbulent viscosity.

VI.B.1. Half-sphere roughness element

First, the spherical roughness element has been considered since several experimental investigations have been carried out on such a geometry. Morrisette[22] shows some interesting results of the flow downstream of an half-spherical roughness element with an interpretation of flow topology as it is represented in Fig. 17. In Fig. 18(a), the skin friction lines and contours obtained with the numerical simulation are represented showing agreement with the experimental data of Morrisette.[22] In Fig. 18(b), velocity streamlines are shown on the plane of symmetry showing two couples of counter rotating vortices in agreement with the interpretation of Morrissette who inferred the presence of a separated region in front of the roughness element.

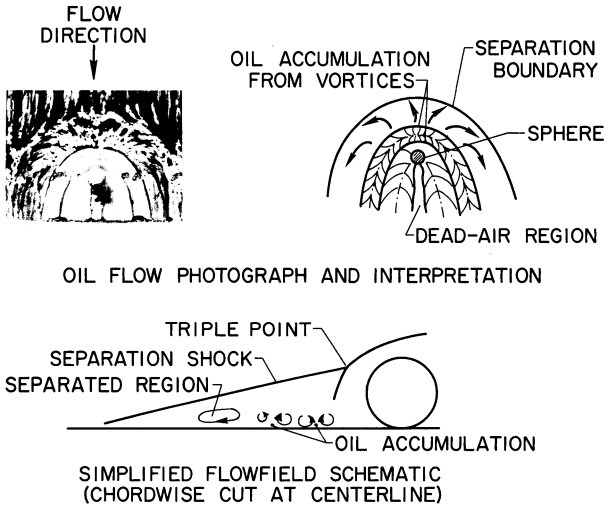

Figure 17. Flow field about spherical element - Reproduced from Morrisette et al.(1969)[22]

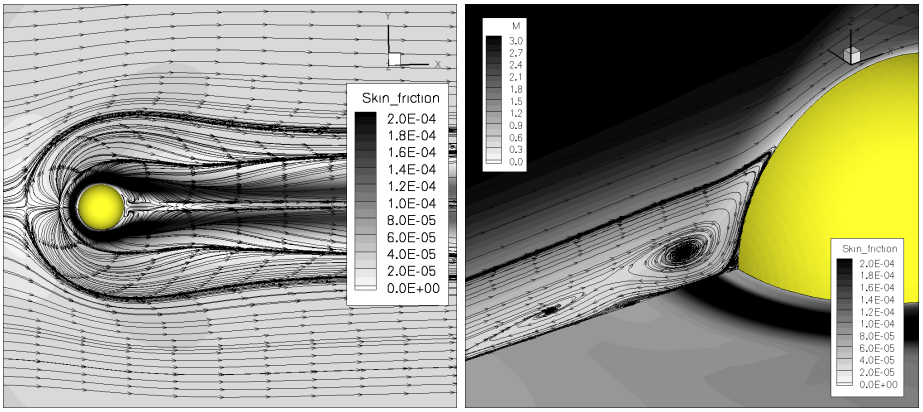

(a) Skin friction lines and contour

(b) Streamlines (symmetry plane) and Mach number, skin Friction contour

Figure 18. Spherical roughness element : flow topology

A qualitative comparison with experimental data obtained by Tirtey[8] in the VKI H3 facility was also performed as represented in Fig. 19 and Fig. 20 respectively for the heat flux and the skin friction coefficient. The flow topology at the roughness element is very close to the experimental one and in the central part of the wake, where the footprint of the primary generation of vortices can be clearly distinguished. As for the ramp element, the secondary generation in the experiment is not captured, resulting in a narrow wake.

Figure 19. Heat flux experimental(bottom)-numerical(top) distributions comparison : half sphere

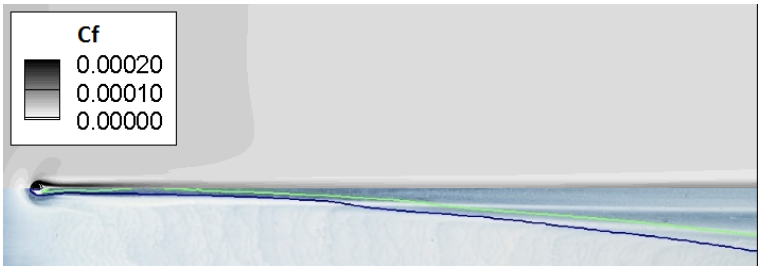

Figure 20. Skin friction experimental(bottom)-numerical(top) distributions comparison : half sphere

VI.B.2. Cylinder roughness element

Results on the cylinder are represented in Fig. 21, Fig. 22 for the heat flux and skin friction distribution. Since such a geometry has a stagnation point, the effects on the flow is heavier as well as the intensity of the primary and secondary generations of vortices in the wake. Therefore, differences between numerical and experimental heat flux and skin friction distribution are more evident downstream of the obstacles with respect to the spherical and the ramp roughness element. However, in all the cases, when the viscosity ratio is set to $VR = 2$ as initial condition on the inflow, bypass transition is obtained in the wake without natural transition occurring on the flat plate.

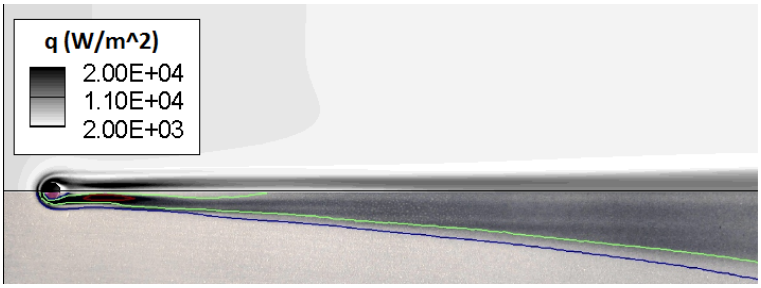

Figure 21. Heat flux experimental(bottom)-numerical(top) distributions comparison : cylinder

VI.B.3. Diamond roughness element

This geometry has the most influence on the flow due to its shape which is characterized by sharp edges and steps both in the front and on the back side of the element. Therefore, even if the topology near the roughness is very close to the experiments, as represented in Fig. 23 and in Fig. 24 for the heat flux and skin friction distribution, differences increase downstream of the transition point.

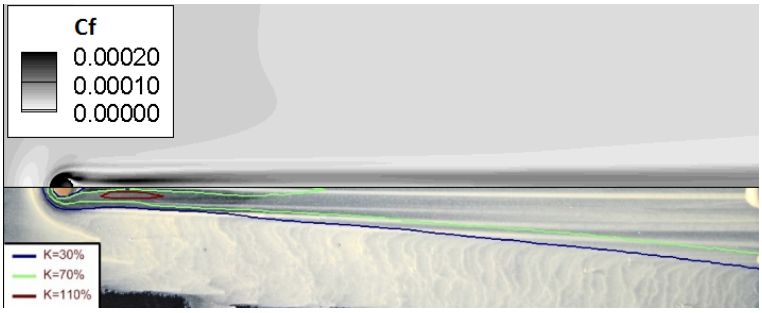

Figure 22. Skin friction experimental(bottom)-numerical(top) distributions comparison : cylinder

Figure 23. Heat flux experimental(bottom)-numerical(top) distributions comparison : square

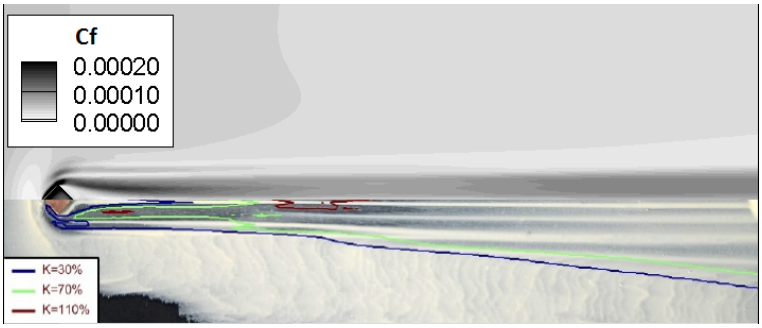

Figure 24. Skin friction experimental(bottom)-numerical(top) distributions comparison : square

VI.B.4. Conclusions on the other geometries

In Fig. 25, the computed skin friction coefficient is represented on the symmetry plane ($y = 0$ mm) as a two dimensional plot immediately behind the roughness location ($x = 65$ mm) until the end of the flat plate. The transition onset abscissa is recognized by the increasing of the skin friction coefficient due to the turbulent flow. The diamond roughness element creates an huge obstacle to the flow since it offers both a stagnation point and a step in the rear part. This promotes the mechanism of transition so that the flow is already turbulent when it reattaches to the wall after the separation right behind the element. The cylinder has also a stagnation point and back step but its rounded geometry allows to avoid separation and to delay transition at $x \approx 100$ mm. The sphere is the element with less effects on the skin friction coefficient since there is no back step and transition is delayed up to $x \approx 140$ mm.

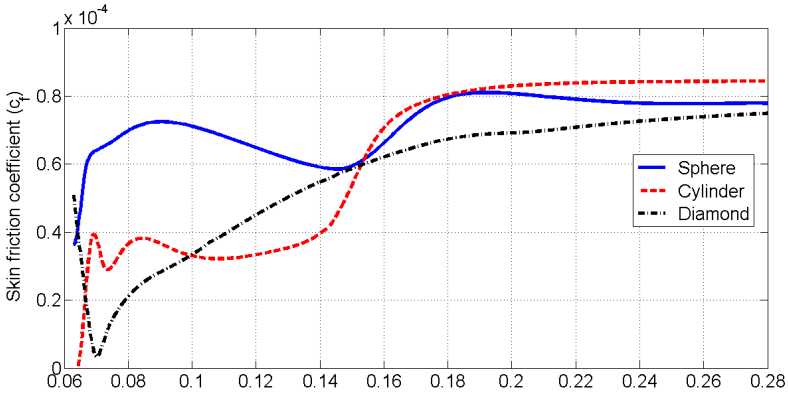

Figure 25. Skin friction coefficient (c_f) for different roughness element : $y = 0$ mm

VII. Conclusion

The objective of the work is to reproduce the onset of transition, heat flux and skin friction previously obtained in experiments in order to enhance our prediction capability for future experiments and extrapolation to flight. Different roughness geometries (ramp, square, cylinder and sphere) were used in the numerical simulations and an overall agreement was achieved in the wake immediately behind the elements. The agreement with experimental data was particularly interesting in the central part of the wake for what concerns the topology, the footprint of the primary generation of vortices and the transition onset location. It was demonstrated through different meshes (6.5×10^6 and 10×10^6) and studies on the parameters of the $R-\gamma$ transitional model, that the second generation of vortices noticed in the experiments is particularly difficult to reproduce. Attempts with a time-resolved approach are currently under investigation.

This work examined the capabilities of the $R-\gamma$ transitional model. A high sensitivity was found concerning the viscosity ratio VR which has to be properly adjusted for each case. For the current cases (see conditions Tab. 2), fully turbulent flow was found for $VR = 4$ while a full laminar flow was obtained for $VR = 1$. Within the interval $VR = 1 \div 4$, the flow is transitional with the transition onset location moving upstream as the viscosity ratio increases. A $VR = 2$ allows to obtain transitional flow in the wake without natural transition on the flat plate closely resembling experimental results. The variation of the intermittency factor γ has no or limited influence on the results while the density of the mesh affected the resolution of the vortices in the outlet plane without affecting the bypass transition onset location.

Overlooking the many limitations of this kind of transition modeling, our work narrowed the choice of the important parameter giving a well defined range of values ready to use in similar simulation. This proves of great help in a first evaluation of the main quantities involved in the phenomenon from an engineering point of view, such as heat flux and skin friction for instance.

References

[1]Reshotko E., Paths to transition in wall layers, Lectures Series in "Advances in laminar-turbulent transition modeling", von Karman Institute for Fluid Dynamics, 2008.

[2]White F.M., Viscous Fluid Flow, McGraw-Hill, New York, 1974.

[3]Schlichting H., Boundary Layer Theory, Springerlink 1965.

[4]Morkovin M.V., The Many Faces of Transition. In Viscous Drag Reduction, Wells, C.S. editor Plenum Press (1969).

[5]Ergin F.G. and White E.B., Unsteady and Transitional Flows Behind Roughness Elements. AIAA Journal, 44(11):2504-2514 (2006).

[6]Chau-Lyan Chang, Meelan M.Choudari,Fei Li, Numerical Computations of Hypersonic Boundary Layer over Surface Irregularities, 48th Aerospace Science Meeting, January 2010, Orlando, Florida.

[7]A.Marino, R.Fauci, Hypersonic Laminar-Turbulent Transition Experiment Design : from Wind-Tunnel model definition to MDOE Approach, 48th Aerospace Science Meeting, 2010, Orlando, Florida, January

[8]S.C.Tirtey, O.Chazot,L.Walpot, Characterization fo hypersonic roughness-induced boundary-layer transition, Von Karman Institute of Fluid Dynamics, PhD Thesis, 2010.

[9]S.C.Tirtey, In flight hypersonic roughness induced transition experiments, 46th AIAA Aerospace Science Meeting, VKI PR 2008-25.

[10]S. A. McKeel. Numerical simulation of the transition region in hypersonic flow. PhD thesis, Virginia Polytechnic Institute, 1996.

[11]Harris J. Warren E. and Hassan H., A Transitional Model for High Speed Flow, AIAA-94-1851-CP, 1994.

[12]K. Sieger, R. Schiele, F. Kaufmann, S. Wittig, and W. Rodi. A two-layer turbulence model for the calculation of transitional boudnary layers. In ERCOFTAC Bullettin, number 24. 1995.

[13]R. B. Langtry. A Correlation-Based Transition Model using Local Variables for Unstructured Parallelized CFD codes. PhD thesis, Stuttgart University, 2006.

[14]R. E. Mayle and Schulz. The path to predicting bypass transition. ASME Journal of Turbomachinery, 119:405411, 1997.

[15]D. K. Walters and J. H. Leylek. A new model for boundary layer transition using a single point rans approach. In ASME IMECE 2002, number HT-32740, 2002.

[16]Ryong Cho, Ji and Kyoon Chung, M., A $k-\epsilon$ Equation Turbulence Model, Journal of Fluid Mechanics, 1992, vol.237, pag.301-322

[17]CFD++ User Manual, Metacomp Technologies, 2010

[18]Goldberg U., Turbulence Closure with a Topography-Parameter-Free Single Equation Model, International Journal of Computational Fluid Dynamics, 2003, vol.17, pag.27-38

[19]Spalart,P.R. and Allmaras,S.R., A one equation turbulence model for aerodynamic flows, American Institite of Aeronautics and Astronautics (AIAA), 1992, vol.92-0439

[20]A. Haas. Assessment and Validation of Intermitency Transport Equations for Modeling Hypersonic Transition with COOLFluid and CFD++. VKI PR 2010-12, von Karman Institute for Fluid Dynamics, 2010.

[21]G.K. Batchelor. An Intoduction to Fluid Dynamics. Cambridge University Press, 1967.

[22]Morrisette E.L., Stone D.R and Cary A.M.Jr., Downstream effects of boundary layer trips in hypersonic flow, NASA Langley Research Center, 1969.